Communications with Mars During Periods of Solar Conjunction: Initial Study Results

D. Morabito[1] and R. Hastrup[2]

During the initial phase of the human exploration of Mars, a reliable communications link to and from Earth will be required. The direct link can easily be maintained during most of the 780-day Earth–Mars synodic period. However, during periods in which the direct Earth–Mars link encounters increased intervening charged particles during superior solar conjunctions of Mars, the resultant effects are expected to corrupt the data signals to varying degrees. The purpose of this article is to explore possible strategies, provide recommendations, and identify options for communicating over this link during periods of solar conjunctions. A significant improvement in telemetry data return can be realized by using the higher frequency 32 GHz (Ka-band), which is less susceptible to solar effects. During the era of the onset of probable human exploration of Mars, six superior conjunctions were identified from 2015 to 2026. For five of these six conjunctions, where the signal source is not occulted by the disk of the Sun, continuous communications with Mars should be achievable. Only during the superior conjunction of 2023 is the signal source at Mars expected to lie behind the disk of the Sun for about one day and within two solar radii (0.5 deg) for about three days.

I. Introduction

During the initial phase of the human exploration of Mars, a reliable communications link to and from Earth will be required. The direct link can easily be maintained during most of the 780-day Earth–Mars synodic period. However, during periods in which the direct Earth–Mars link encounters increased intervening charged particles during superior solar conjunctions of Mars, these effects are expected to corrupt the data signals to varying degrees.

During superior solar conjunctions of interplanetary space probes, flight projects routinely downscale their operations. This involves invoking command moratoriums, reducing tracking schedules, and lowering data rates. The actual detail varies between flight projects and from conjunction to conjunction. The solar conjunction periods are also used by flight projects as an opportunity to study the effects of solar charged particles on the communications links.

---

[1] Communications Systems and Research Section.

[2] Mission and Systems Architecture Section.

The research described in this publication was carried out by the Jet Propulsion Laboratory, California Institute of Technology, under a contract with the National Aeronautics and Space Administration.

The Near Earth Asteroid Rendezvous (NEAR) spacecraft underwent a superior conjunction in early 1997 when its distance from the Earth was 3.17 au. The link frequency was 8.4 GHz (X-band), and the downlink utilized an inner (7,1/2) convolutional code with an outer Reed–Solomon code. An engineering experiment, which analyzed the telemetry error statistics as a function of solar elongation or Sun–Earth–Probe (SEP) angle, was conducted and reported on in [1]. The results of this study will be briefly summarized here. Figure 1 displays the downlink telemetry frame error rate for the 1997 NEAR solar conjunction.

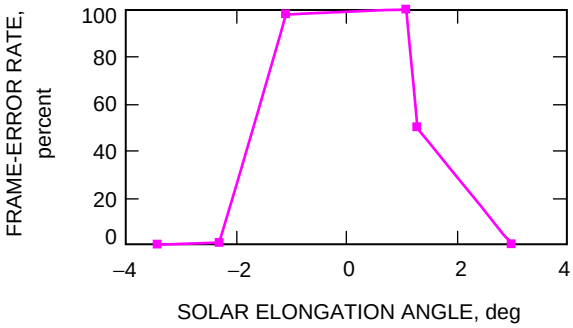

Fig. 1. Frame-error rate versus solar elongation angle during NEAR 1997 solar conjunction.

Note that for the NEAR conjunction, for passes conducted above SEP angles of 2.3 deg, the frame error rate was near zero. At SEP angles of 2.3, 3.0, and 3.4 deg, the frame success rate was 99.7, 100, and 100 percent, respectively, using a 1104-b/s data rate. At an SEP angle of 1.3 deg, the frame success rate was 54 percent using a 39.4-b/s data rate. At SEP = 1.1 deg, the frame success rate became significantly reduced to 3 percent at $R = 1104$ b/s and 0 percent at $R = 39.4$ b/s. For reference, the predicted downlink telemetry margins were 6 dB for 1104 b/s and 19 dB for 39.4 b/s in the absence of solar effects. In the region of weak scintillation, NEAR achieved nearly perfect frame recovery, while near the expected transition to strong scintillation (at 1.3 deg), partial success was achieved (46 percent frame error rate), and, in the realm of strong scintillation, a very low percentage at or near zero frames was received.

The NEAR spacecraft also conducted an uplink test at X-band in which a series of commands was radiated to the spacecraft and the percent successfully received by the spacecraft was tabulated as a function of SEP angle [1]. The uplink command bit rate was 125 b/s, and the predicted uplink command margin was 29 dB in the absence of solar effects. For angles above 2.4 deg, almost all commands sent were received. The loss of those few commands, which were not successfully received, was attributed to a command detector unit (CDU) anomaly. If these are discarded, a 100 percent success rate was achieved. For SEP angles $\leq$1.3 deg, significantly fewer commands ($\sim$14 percent) were successfully received.

Based on this work, one should expect reasonable data return at SEP angles above 2.3 deg at X-band, neglecting the effects of any possible significant solar transient events. Between 2.3 and 1.3 deg, one should expect increased degradation as the region of strong scintillation is approached. Below 1.3 deg, in the realm of strong saturation, the effects will be severe.

Using analytical and simulation techniques, Feria et al. [2] demonstrated that an X-band link, for the example of a solar probe geometry, should suffer an 8.2-dB degradation while the corresponding 32-GHz (Ka-band) link should suffer only a few tenths of a dB loss (bit-error rate = 10^{-5}). This result assumed a scintillation index (m = the ratio of the rms of intensity fluctuations due to solar charged particles to the mean intensity) of $m = 0.37$ at X-band, corresponding to an SEP angle of 1 deg. At an SEP angle of 2 deg, $m = 0.099$, and the degradation fell to 0.4 dB at X-band. For typical solar conjunction geometries, these results can be extrapolated to other SEP angles using known scintillation models.

For Galileo, which used the much lower downlink frequency of 2.3 GHz (S-band), reliable telemetry was not possible for SEP angles below 4 deg [3]. Uplink command tests were performed during the Galileo solar conjunction in October and November of 1993 for SEP angles ranging from 8.5 to 1.2 deg. These tests showed that the CDU lockup was intermittent and unstable for SEP angles below 3.9 deg at S-band [3]. It should be emphasized that the Galileo low-gain antenna (LGA) mission used very low bit rates with very low margins.

II. Effects Of Charged Particles and the Solar Disk on Signals

The effects of solar charged particles on spacecraft signal links include scintillation, or fades, impressed on the carrier and subcarrier amplitude as the signals propagate through the solar charged particles. These fades can produce significant degradation of the received signals as the SEP angle decreases. This will severely affect carrier and data channel lock as well as symbol detection. For normal superior conjunction geometry, the amplitude is expected to saturate at SEP angles near 1.25 deg at X-band[3] and near 0.67 deg at Ka-band [4]. The actual scintillation effect measured will depend on conditions such as presence of solar events, phase of the solar cycle (solar maximum versus solar minimum), and the sub-solar latitude of the observations.

Spectral broadening refers to an increase in the signal bandwidth, B, due to charged particles. This quantity is dependent on both electron density fluctuations and solar wind velocity, whereas the intensity scintillation index depends only on the electron density fluctuations. Since B does not saturate with decreasing SEP angle, it is useful for detecting the effects of solar transients or features near the Sun. Spectral broadening is useful only when the observations are conducted close enough to the Sun such that the broadening exceeds the oscillator line width. Since spectral broadening measurements are valid for bandwidths larger than $\sim$0.02 Hz, it is similar to intensity scintillation, which responds only to small scale sizes. A Ka-band link will have a measured spectral broadened bandwidth of only one-fifth that of a simultaneous X-band link at the same SEP angle [4], assuming the broadening exceeds the oscillator line width for both bands.

The measure of phase scintillation provides information on the full range of scale sizes as opposed to intensity scintillation and spectral broadening, which are responsive only to small scale sizes. Phase fluctuations do not saturate, as is the case with intensity scintillation. One measure of phase scintillation is Doppler noise, the scatter of frequency residuals in which long period trends due to non-solar effects are removed from the frequency data using a trajectory or polynomial fit. The Doppler scintillation parameter, σ_D, which is analogous to intensity scintillation, is the rms of the Doppler over a 10-minute time span (600 s) for data sampled at one per 60 s [5]. The Doppler noise depends on charged-particle relative velocity, v, and density fluctuations as opposed to intensity scintillation, which is sensitive only to density fluctuations.

In addition to the above effects, a signal link approaching the limb of the Sun will exhibit significantly increased thermal noise as the antenna pattern side lobes start to pick up significant contributions of the solar disk temperature. Solar-temperature increase profiles of 34-m and 70-m antennas versus SEP angle are available in [6]. A comprehensive study of measured noise-temperature increases near and on the Sun for a 34-m beam-waveguide (BWG) antenna was conducted by Otoshi [7]. As one tracks a signal source near the solar disk, the temperature changes will be significant due to antenna pattern side lobes sweeping in and out of the solar disk [8]. The system temperature increase due to the Sun with the use of a 34-m antenna at Ka-band is about 80 K with several K variation depending on conditions.

---

[3] J. Armstrong and R. Woo, "Contribution to Starprobe Report," JPL Interoffice Memorandum 3331-80-070 (internal document), Jet Propulsion Laboratory, Pasadena, California, December 15, 1980.

III. Mars Solar Conjunction Geometry

During Mars–Sun–Earth superior conjunctions (Fig. 2), the Sun lies between the Earth and Mars. It is during this period that the Earth–Mars distance is at or near maximum and the received signal strength is at its weakest level. In addition, the intervening charged particles of the solar corona in the signal path produce significant amplitude scintillation, phase scintillation, and spectral broadening effects, which increase as the Sun–Earth–Mars (SEM) or "solar elongation" angle decreases. For the return link, in which the element at Mars transmits and the element at Earth receives, the visible surface of the Sun, or photosphere, appears as a disk 0.264 deg in radius as seen from the receiving antenna on Earth. For the forward link, in which the element at Earth transmits and the element at Mars receives, the visible surface of the Sun appears as a disk 0.175 deg in radius as seen from the receiving antenna on Mars. In each case, the receiving pattern of the antenna against the disk picks up significantly increased thermal background noise as the solar elongation angle decreases.

During inferior solar conjunctions (Fig. 3), the Earth lies between the Sun and Mars. It is during this period that the Earth–Mars distance is at or near minimum and the received signal strength is at its strongest level. In addition, the intervening charged particles of the solar wind that lie in the signal path between Earth and Mars are significantly less dense than in the superior conjunction case, and the resulting scintillation and broadening effects are expected to be small to negligible. For the return link, in which the element at Mars transmits and the element at Earth receives, the source (Mars) appears in the night sky at opposition as seen from the receiving antenna on Earth. Therefore, this link is expected to perform at its best since the signal strength will be at or near maximum and the noise will be near its minimum (neglecting weather effects on Earth). For the forward link, in which the element at Earth transmits and the element at Mars receives, the visible surface of the Sun appears as a disk 0.175 deg in radius as seen from the receiving antenna on Mars. In this case, the side lobes of the antenna pattern that fall on the disk of the Sun pick up significantly increased contributions of thermal noise as the solar elongation angle decreases.

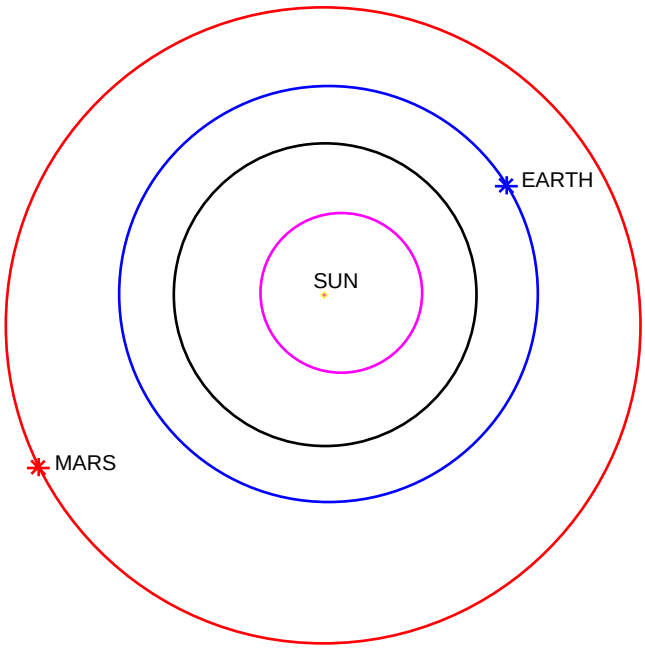

Fig. 2. Mars—Sun—Earth superior conjunction geometry with orbits of the inner planets shown.

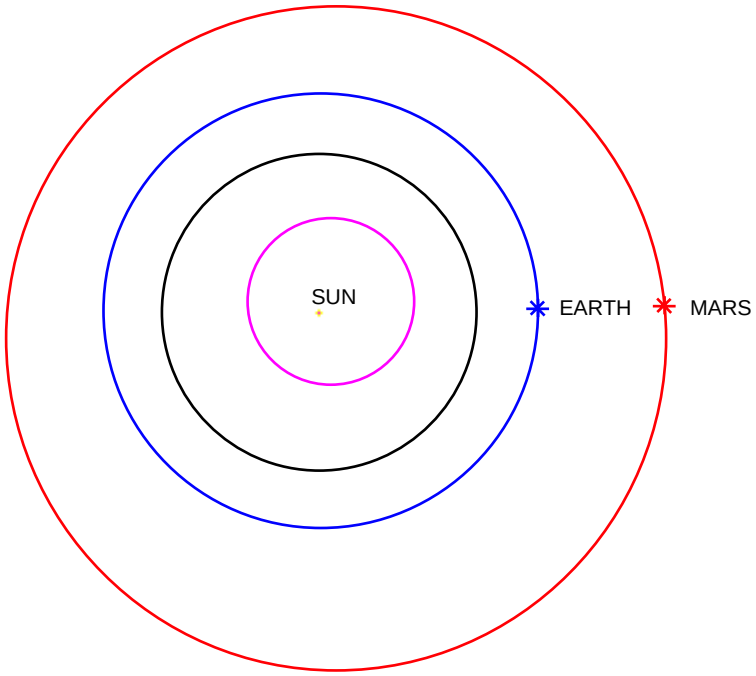

Fig. 3. Sun—Earth—Mars inferior conjunction geometry with orbits of the inner planets shown.

During the era of the onset of probable human exploration of Mars, six superior conjunctions were identified from 2015 to 2026, as summarized in Table 1. During the periods around these superior conjunctions, direct communication with Mars is expected to deteriorate as the angle of the signal source relative to the center of the Sun decreases. Table 1 lists the minimum SEM and Sun–Mars–Earth (SME) angles that are expected during each conjunction. Only during the 2023 superior conjunction is the signal source at Mars expected to lie behind the disk of the Sun for about one day and within two solar radii (0.5 deg) for about three days. In all other cases, the minimum angle is greater than the disk size of the Sun.

Profiles of the SEM and SME angle variation with time are shown in Fig. 4 for the six conjunctions. Also shown on these plots are the 0.264-deg disk radius of the Sun as seen from the Earth and the 0.175-deg disk radius of the Sun as seen from Mars. When the SEM angle falls below 0.264 deg, the signal source is behind the Sun as seen from Earth. Similarly, when the SME angle falls below 0.175 deg, the signal source is behind the Sun as seen from Mars.

Table 1. Mars–Sun–Earth superior solar conjunction characteristics.

Conjunction date	Minimum SEM angle, deg	Minimum SME angle, deg	Expected solar cycle phase	Passage
June 14, 2015	0.62	0.40	Minimum	Northern polar
July 27, 2017	1.10	0.68	Rise	Northern polar
September 2, 2019	1.08	0.66	Rise	Northern polar
October 8, 2021	0.65	0.40	Maximum	Northern polar
November 18, 2023	0.11	0.08	Maximum	Ecliptic
January 9, 2026	0.94	0.66	Minimum	Southern polar

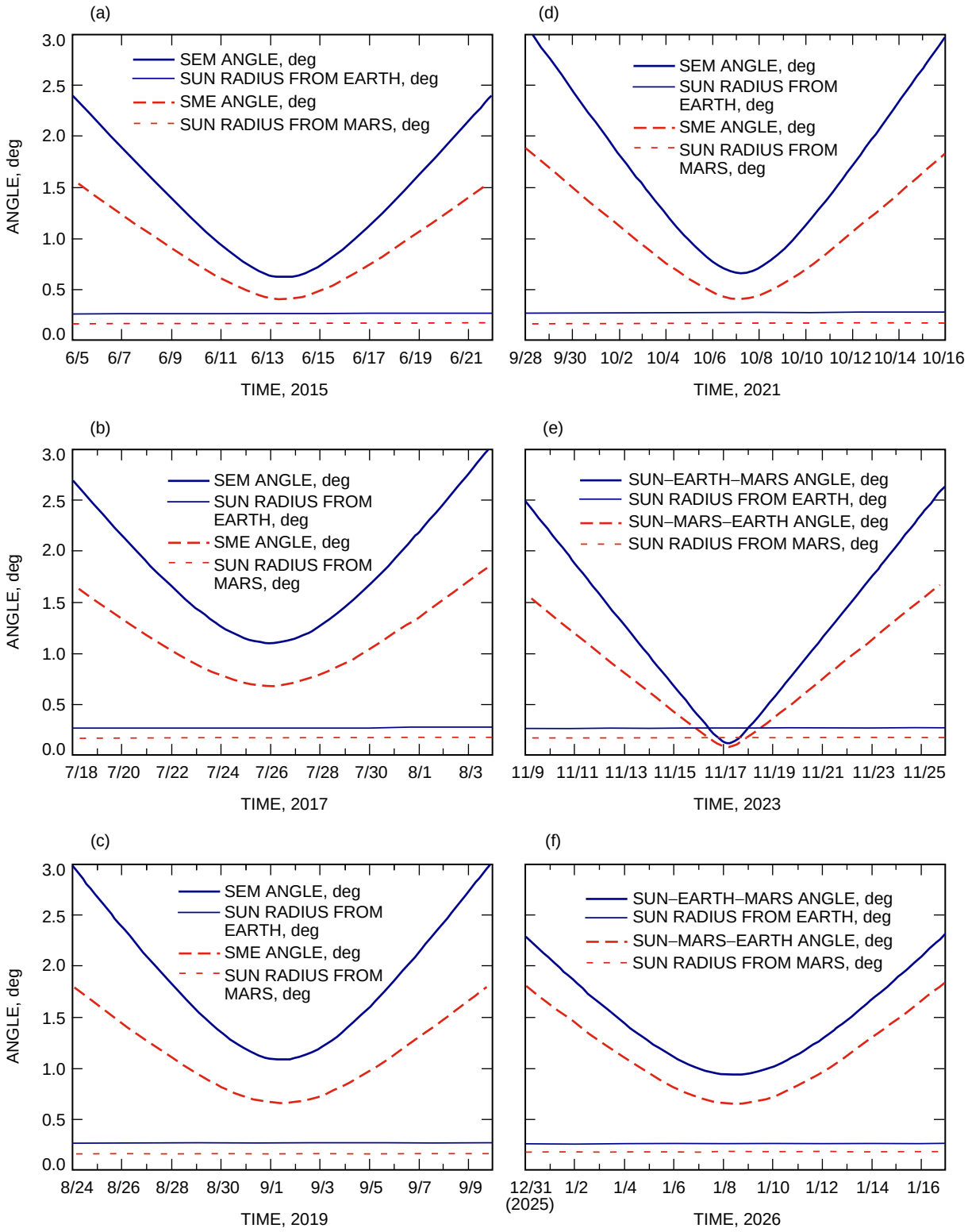

Fig. 4. Superior conjunction SEM and SME angles: (a) 2015, (b) 2017, (c) 2019, (d) 2021, (e) 2023, and (f) 2026.

The trajectory of Mars in the vicinity of the Sun as seen from Earth is displayed in Fig. 5 for each solar conjunction listed in Table 1. The 2023 superior conjunction, which is an ecliptic passage of Mars behind the Sun, is the only one of the six conjunctions when Mars becomes occulted for about a day. All other passages are polar passages, where the minimum SEM angle lies above a polar region of the Sun.

In addition to the angle from the Sun's center, the location of the source relative to solar latitude is important to consider, depending upon the phase of the solar cycle. During solar maximum conditions, solar activity can occur anywhere off of the solar disk and, thus, spacecraft at any solar latitude should experience similar effects at a given SEP angle. During solar minimum conditions, solar activity is constrained primarily in the low solar latitudes, and the regions above the poles should be very quiet. At a given solar elongation angle, those conjunctions in which the source passes above or below the Sun should display improved communication links during a solar minimum as opposed to those during solar maximum. Those conjunctions in which the source passes through the low solar latitude regions should display

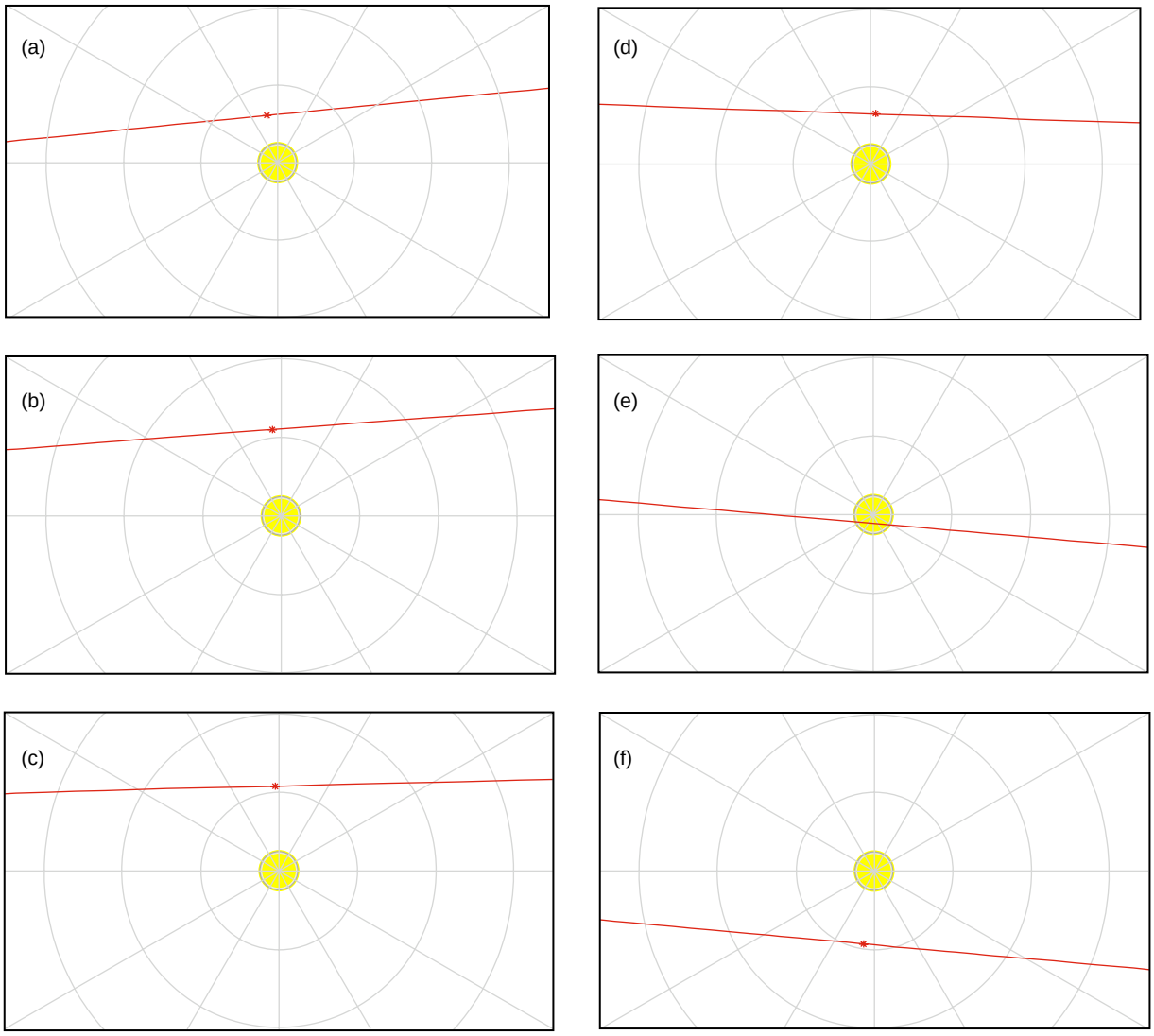

Fig. 5. Mars solar conjunction trajectories superimposed against the solar disk as viewed from Earth: (a) June 14, 2015, (b) July 27, 2017, (c) September 2, 2019, (d) October 8, 2021, (e) November 18, 2023, and (f) January 9, 2026. Note: circles are at 1-deg increments.

conditions that are just as noisy during either solar maximum or solar minimum conditions. Figure 6 displays a plot of solar activity, as measured by the number of sunspots[4] for solar cycle no. 23. Also indicated on Fig. 6 are the approximate predicted locations of the martian solar conjunctions listed in Table 1 with respect to solar cycle phase. It is stressed that these predictions are based on an extrapolation of the present solar cycle using a fixed 11-year solar cycle period. Extrapolating the solar cycle into the future for prediction purposes should be treated with caution, as the uncertainty grows as one extrapolates further into the future.

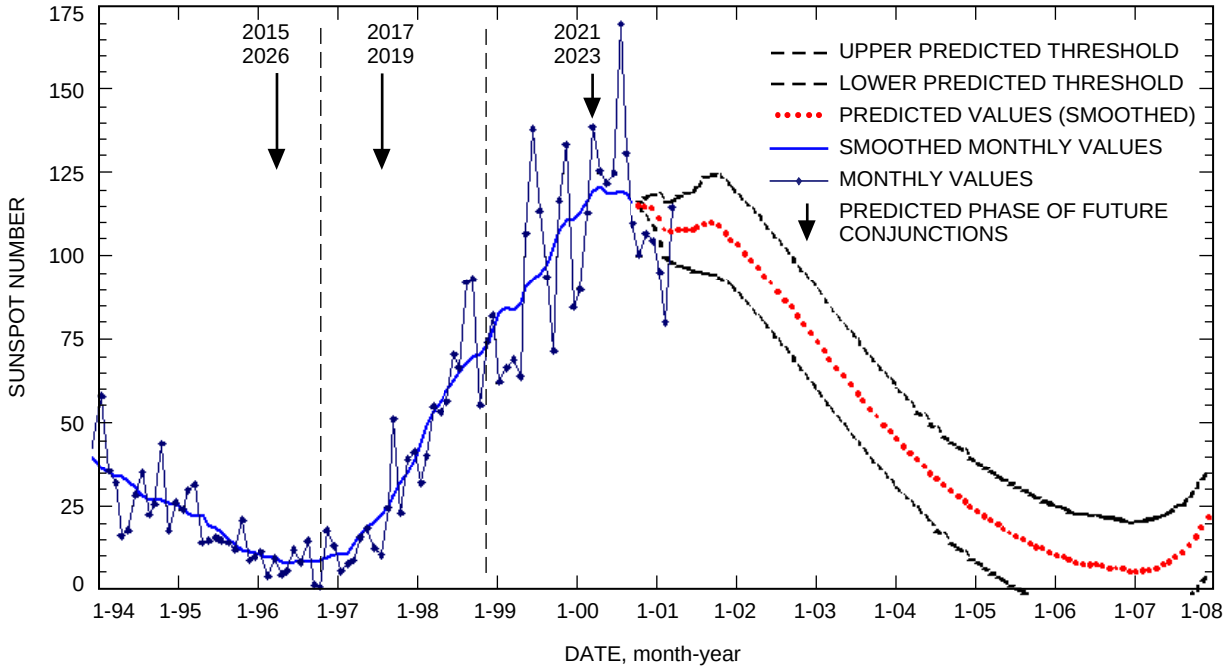

Fig. 6. Plot of solar cycle no. 23 sunspot number along with the predicted phase of future Mars solar conjunctions using an extrapolation of 11-year cycle.

IV. Strategy in the Realm of Weak Scintillation

When tracking a spacecraft at an angular distance far from the Sun, where the scintillation effects due to charged particles are minimal (scintillation index, $m < 0.2$), routine operations should suffice. Depending upon SEP angle, additional margin can be added to the link budgets to account for expected thermal noise contributions, using existing models as a function of SEP angle.

Since NEAR was able to obtain 100 percent downlink frame return with adequate margins down to an SEP angle of 2.3 deg at X-band during the 1997 solar conjunction, one expects that similar success should be achievable at Ka-band down to an SEP angle of 1 deg. This is based on examination of measured scintillation index versus SEP for both X-band and Ka-band from the Cassini 2000 solar conjunction [9] carrier data, which have been superimposed upon solid-curve scintillation models for both bands in Fig. 7. Thus, upon examination of Fig. 7, the successful NEAR results that were achieved for SEP angles down to 2.3 deg, corresponding to a scintillation index $\sim$0.3, imply that similar success should be achieved using Ka-band for SEP angles down to 1 deg.

[4] Plot created by U.S. Department of Commerce, National Oceanic and Atmospheric Administration (NOAA), Space Environment Center (Web site at http://sec.noaa.gov).

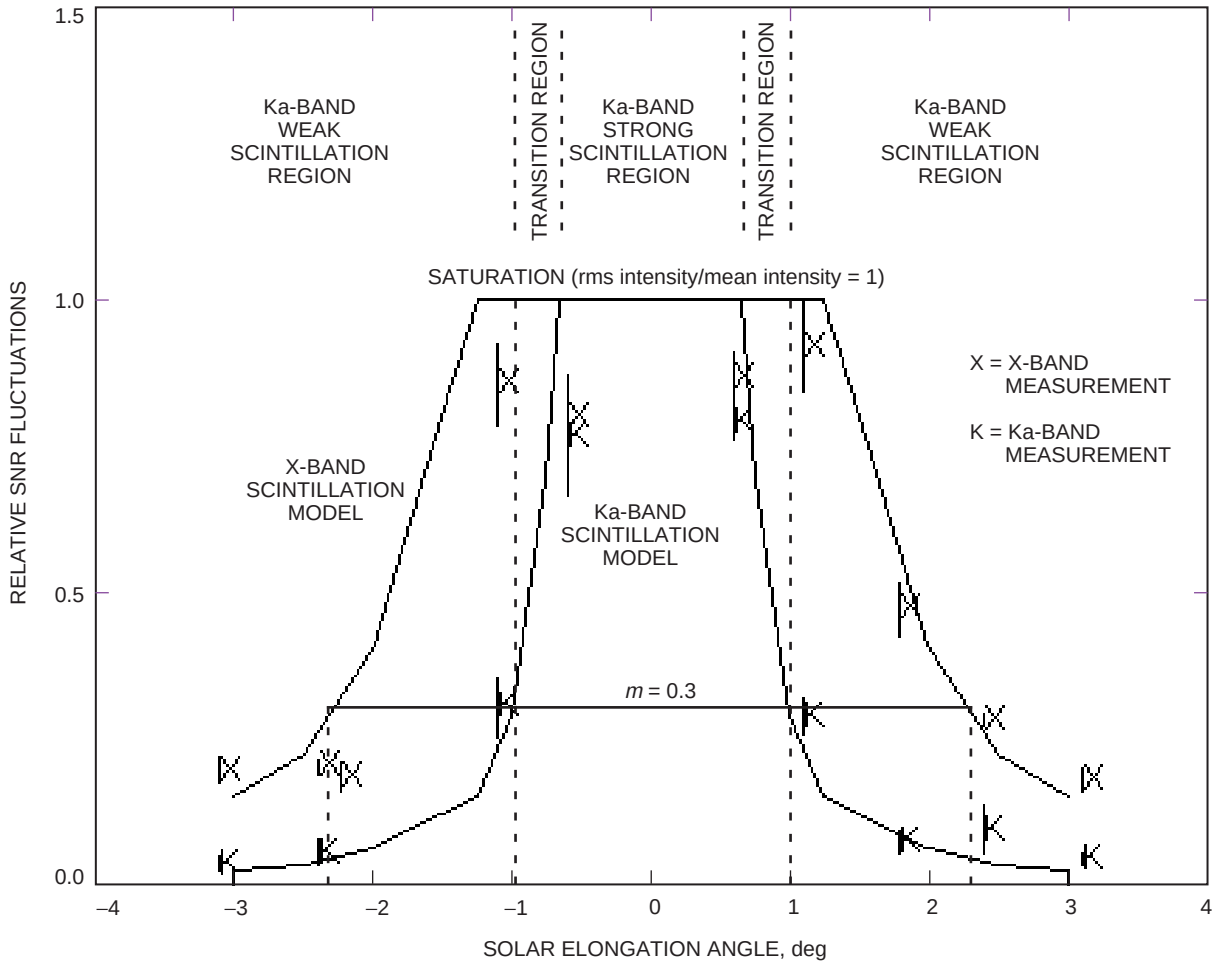

Fig. 7. Cassini 2000 solar conjunction relative SNR fluctuations. Note that the relative fluctuations of the SNR are equivalent to the scintillation index, *m*, when the fluctuations are dominated by solar plasma.

Feria et al. [2] showed that an 8-dB degradation at $m = 0.37$ is expected at X-band. This case was for a solar probe geometry at a 1-deg SEP angle. If we assume that these results can be extrapolated for a normal solar conjunction geometry such as for Mars, then this result is consistent with the NEAR 1997 X-band case using binary phase-shift keying (BPSK), where at least 6 dB of margin were available for SEP angles above 2.3 deg and $m \lesssim 0.3$. From Fig. 7, the Ka-band model at $m = 0.3$ occurs at an SEP angle close to 1 deg. Thus, one may assume that similar success should be achievable using BPSK at Ka-band for SEP angles above 1 deg.

V. Strategy in the Transition Region

For SEP angles in the Ka-band weak-to-strong scintillation transition region from 1 deg down to the expected saturation point at about 0.67 deg, it will become harder and harder to maintain telemetry lock using phase-shift keying (PSK) modulation. Presumably, with sufficient margin, a partial degree of successful telemetry return using BPSK could be achieved as one moves further in from 1 deg to somewhere close to 0.7 deg and m increases from 0.3 to somewhere just before saturation ($m = 1$). This needs to be quantified as a function of margin to counter deep fades, as NEAR showed a partial return with limited margin in the X-band transition region. This is an appropriate focus for further study. However, it is recommended that the transition region be treated in the same way as the realm of strong saturation discussed in the next section.

VI. Strategy in the Realm of Strong Scintillation

When the signal source is very near the Sun in angular distance, the received signal is expected to exhibit severe amplitude scintillation and spectral broadening effects due to increased charged-particle densities and turbulence. Strategies for countering such effects and optimizing data return are discussed here.

During periods of strong scintillation, PSK signals may become hopelessly corrupted. Scintillation causes rapid signal changes, which may not permit coherent or accurate carrier phase tracking. For very small SEM angles, the amplitude saturates such that rms $(P_c/N_o) \approx$ mean (P_c/N_o). There are challenges to designing a BPSK link under such conditions. A scheme that spreads the bits over frequency space may prove to be more conducive in optimizing data return. Non-coherent frequency-shift keying (FSK) may provide improved data return under conditions of strong scintillation. Coherent detection is not essential if the signal-to-noise ratio (SNR) is sufficiently strong. Therefore, non-coherent FSK detection could be a viable recourse.

The achievable data rate using FSK, given an available P_c/N_o and a broadened bandwidth, needs to be carefully evaluated for different SEP angles. Integration of signal power over fades may determine viable data rates. The expected fade duration and fade magnitude should also be considered. If the bit period is comparable to the fade duration ($T_B \sim T_F$), there may be bursts of errors that could be countered with redundancy. If $T_B > T_F$, we could average over the fades at the cost of using a lower data rate than what the link could otherwise support.

Non-synchronous semaphores can be considered when a reference carrier is used that is suppressed. The use of semaphores differs from FSK in that one frequency is transmitted for a given time period until some condition changes. Semaphores perform better at low P_c/N_o than do FSK signals. A simple semaphore strategy uses two tones on each side of the carrier frequency. Received frequencies are expected to be well known using ultra-stable oscillator (USO), or better, signal references and adequate trajectory modeling. The period of the semaphore for reasonable detection, T_B, depends on received SNR, broadened bandwidth, fade duration, and fade depth.

During periods of strong scintillation due to solar charged particles, diversity options can also be considered. Given that the scale size of the charged-particle density irregularities are small (∼50 km at X-band, ∼27 km at Ka-band) compared to the radius of the Earth (6378 km), spatial diversity can be exploited using multiple ground antennas. The antennas can be placed far enough apart to exceed the scale size of density irregularities. Thus, deep fade fluctuations will not be correlated between receiving antennas that are simultaneously tracking the signal source.

Another option for conducting communications during solar conjunction is the use of frequency diversity. For the case of weak scintillation, the correlation bandwidth is comparable to the link frequency. Given that the transition to the strong scintillation ($0.5 < m < 1$) region for Ka-band coincides with the strong scintillation region for X-band, frequency diversity is not a viable option here. Here, Ka-band is the preferred frequency link, using other techniques such as FSK or spatial diversity to mitigate fades. In the transition to the strong scintillation ($0.5 < m < 1$) region for X-band, scattering is negligible at Ka-band, so it is practical to transmit the data at Ka-band only. For the case of strong scintillation in both bands, the correlation bandwidth at Ka-band can be estimated using a formula given by Rickett [10]. Assuming an SEP angle of 0.6 deg and Kolmogoroff spectrum, the correlation bandwidth at Ka-band is estimated to be about 260 MHz. Thus, for Ka-band, amplitude fluctuations are expected to be largely uncorrelated over bandwidths exceeding 260 MHz (ideally >>260 MHz), in which case frequency diversity potentially could be useful. The frequency diversity option involves a cost of splitting the available power between the two data channels. Thus, a trade-off exists between losing about 3 dB of margin versus possibly gaining back additional data bits lost due to fades on one frequency that may not be significant on the other frequency. This option merits further study and demonstration.

An example of received Ka-band carrier signal strength versus time is given in Fig. 8 for an SEP angle of about 0.60 deg. These data should be characteristic of the worst-case Ka-band carrier signal behavior for all solar conjunctions listed in Table 1 (except 2023), where the minimum SEM angle is 0.62 deg. These data were acquired during the Cassini June 2001 solar conjunction as Cassini traversed the southern polar region of the Sun's corona, which was close to the minimal SEP angle for this conjunction. It is interesting to note that the data of Fig. 8 were acquired during egress where Cassini was initially in the realm of strong saturation for Ka-band (SEP $<$ 0.67 deg) and then transitioned into the region of weak scintillation (SEP $>$ 0.67 deg). The X-band carrier data, which were simultaneously acquired, were in saturation the entire period.

For comparison with received signal strength profiles at other SEP angles, see Fig. 9 for both X-band and Ka-band SNR, obtained during the Cassini May 2000 solar conjunction [9]. The long-term variations of the Ka-band SNR in Fig. 9 are due to spacecraft dead-banding, resulting from thruster control during the May 2000 solar conjunction. In all cases, the Ka-band SNR scatter (or fluctuations due to solar scintillation) lies below that of the simultaneous X-band SNR data. Note that the scatter of the Ka-band SNR at the higher SEP angles in Fig. 9 is significantly reduced as compared to the Ka-band SNR scatter of the SEP = 0.6-deg case depicted in Fig. 8.

Upon inspection of the Ka-band spectral-broadening measurements for the Cassini pass on June 7, 2001, a worst-case $B = 2.6$ Hz due to spectral broadening was observed. The Cassini 2000 solar conjunction measurements showed similar spectral broadening at 0.6 deg with a maximum $B = 23$ Hz observed during a solar transient event at Ka-band [9].

A link budget covering the case for an SEP angle of 0.6 deg at 32 GHz from Mars to Earth is summarized in Table 2, which takes into consideration the Cassini solar conjunction results discussed above. For this link, we assume that a 200-W RF output power transmitter and a 5-m-diameter transmit antenna are available at Mars. Here the minimal SEP angle of 0.6 deg should be the worst case for all solar conjunctions between 2015 and 2026, except for 2023. Here we account for system temperature increase and broadened bandwidth assuming a 34-m BWG antenna as the receive element at Earth. With 29 dB of margin, we could achieve a worst-case data rate of 948 b/s using Ka-band at the maximum

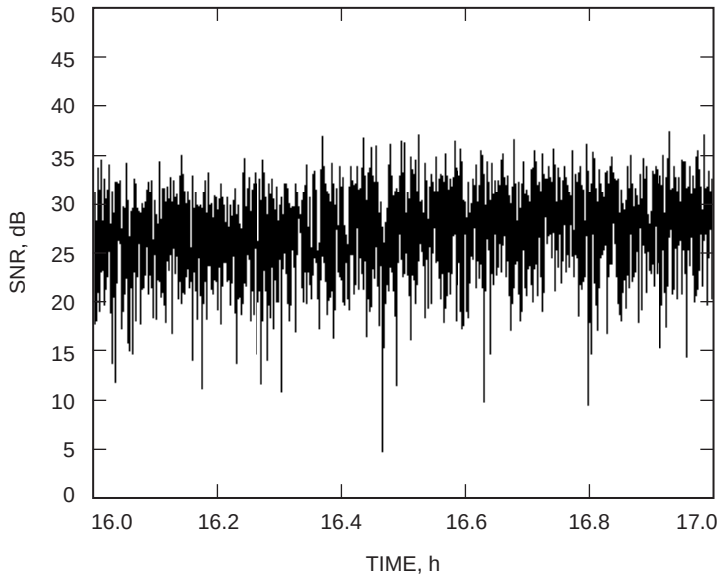

Fig. 8. Cassini Ka-band received carrier SNR, SEP = 0.6 deg, June 7, 2001.

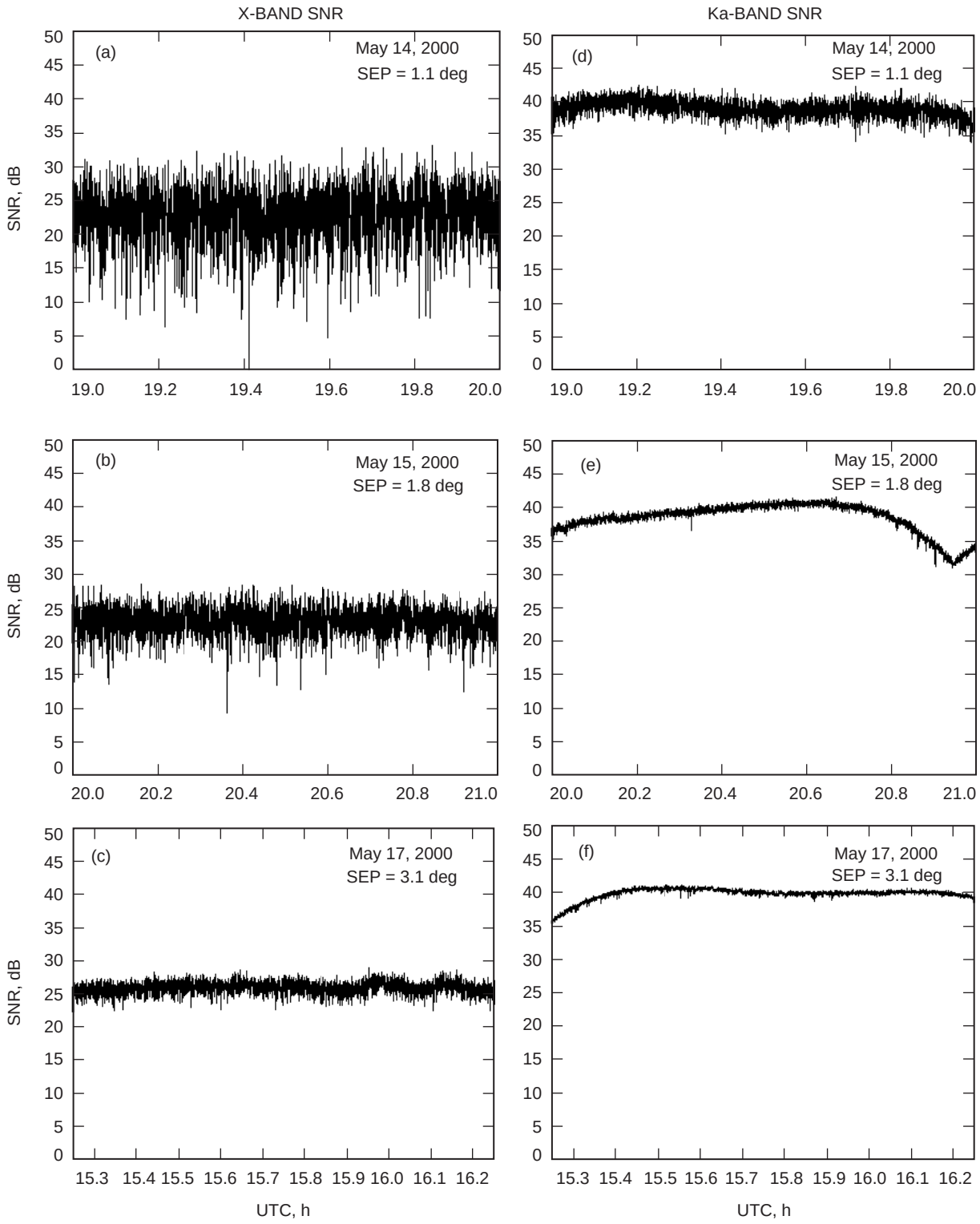

Fig. 9. Cassini 2000 solar conjunction carrier SNR for X-band on: (a) May 14, 2000, at SEP = 1.1 deg, (b) May 15, 2000, at SEP = 1.8 deg, and (c) May 17, 2000, at SEP = 3.1 deg; and for Ka-band on (d) May 14, 2000, at SEP = 1.1 deg, (e) May 15, 2000, at SEP = 1.8 deg, and (f) May 17, 2000, at SEP = 3.1 deg.

Table 2. Mars-to-Earth Earth 34-m downlink performance (SEP = 0.6 deg at 32 GHz).

Parameter	Unit	Ka-band
Spacecraft		
RF transmit power (200 W)	dBm	53.0
Circuit loss	dB	−2.0
Antenna gain (5 m)	dBi	60.5
Pointing loss	dB	−0.5
Effective isotropic radiated power (EIRP)	dBmi	111.0
Path		
Space loss (2.67 au)	dB	−294.6
Atmospheric attenuation	dB	−1.2
Path loss	dB	−295.8
Ground		
Antenna gain (34-m)	dBi	77.7
Microwave circuit loss	dB	−0.0
Pointing loss	dB	−0.2
Total power received	dBm	−107.3
Noise spectral density		
Noise spectral density (120 K at Ka-band)	dBm/Hz	−177.8
Total power-to-noise ratio	dB-Hz	70.5
Carrier performance		
Telemetry suppression	dB	−15.2
Ranging suppression	dB	0.0
Loop bandwidth (10 Hz Ka-band)	dB-Hz	10.0
Carrier loop SNR	dB	45.3
Telemetry performance		
Modulation loss	dB	−0.13
Ranging suppression	dB	0.0
Radio and process loss	dB	−1.0
Decoder threshold (FSK 10^{-3})	dB	10.6
Data rate (948 b/s at Ka-band)	dB-Hz	29.8
Margin	dB	29.0

Earth–Mars range distance of 2.67 au at an SEP angle of 0.6 deg. The 29 dB of margin should cover the effects of the deepest fade in Fig. 8. Higher data rates could be attained as this margin is relaxed using FSK. However, fade-duration effects with smaller symbol periods need to be evaluated, and this is a focus for future work. The addition of coding to achieve higher data rates would be complicated by the fact that shorter symbol periods would be required and need to be assessed against expected fade-duration statistics. The incidence of massive solar transient events such as coronal mass ejections could result in additional complexities. Events such as those seen in Cassini 2000, with increased spectral-broadening bandwidths as high as $B = 23$ Hz, could be mitigated by widening the loop bandwidth to optimize symbol detection. This would also allow more thermal noise in the loop, and this needs to be taken into account in the link with additional margin, as well as margin to counter the large, several-dB fades.

VII. Recommendations

A number of strategies are recommended for optimizing data return over the Earth–Mars direct link for different ranges of solar elongation angle. For X-band, standard downlink BPSK coding strategies can be used to achieve successful data return at SEP angles down to at least 2.3 deg. By going to a higher link frequency (32 GHz), solar effects can be further reduced. Ka-band (32 GHz) is expected to suffer significantly less degradation than X-band, to be less likely to drop lock, and to be more resilient to fades. Previous work studying the solar effects on simultaneous Ka-band and X-band carrier signals during solar conjunctions of Mars Global Surveyor in 1998 [4] and the Cassini spacecraft in 2000 [9] confirm theoretical expectations of the solar effects at these frequencies. The Ka-band carrier suffers 15 percent less amplitude scintillation and 20 percent less spectral broadening than the X-band carrier for the same SEP angle. Earth weather concerns can be addressed with increased margin or ground station diversity.

Given that Ka-band is the preferred link frequency during solar conjunctions, the strategy using Ka-band is the focus of the following discussion.

The use of one-way USO-referenced links instead of two-way or three-way coherent links will result in links free of additional phase effects on any uplink signal, which would be turned around by the spacecraft transponder. These effects would appear on the downlink (multiplied by the transponder ratio). The downlink would also incur its own phase scintillation as well as amplitude scintillation. Thus, the downlink using an on-site oscillator instead of a transponder as the signal source will have significantly fewer solar effects than a downlink signal referenced to an uplink signal. The stability of a USO is more than adequate, as solar effects will dominate at small SEP angles.

The received telemetry data link also can be recorded on an open-loop receiver with a wide enough bandwidth to capture all the symbols. This allows for use of post-data acquisition analysis tools to extract the symbols using a wide variety of signal detection techniques. We could also modulate the carrier directly instead of using a subcarrier. As discussed earlier, we can also consider the use of FSK, semaphores, and/or diversity options in the realm of strong scattering.

The following recommendations are offered for improved link performance using Ka-band during solar conjunctions when the SEP angle is small.

For SEP angles above 1 deg, conduct passes normally, but ensure system noise temperature versus SEP due to solar effects is included in link budgets. Also, widen receiver loop bandwidth to account for increased broadening due to solar transient activity. Select the optimum data rate, coding, and frame size.

For 0.67 deg < SEP < 1 deg, adhere to the above recommendations but also consider use of FSK and/or semaphores. The lower limit may be flexible, depending upon solar conditions at the time. The presence of solar events, the sub-solar latitude, and the phase of the solar cycle should be considered in any strategy.

For 0.4 deg < SEP < 0.67 deg, the realm of strong scintillation (saturation) for Ka-band, adhere to the above recommendations, but also use FSK and/or frequency semaphores with reasonable symbol duration for integration and appropriate spacing in frequency. The benefits of spatial or frequency diversity also should be considered.

For SEP < 0.4 deg, as the SEP angle approaches the disk edge of the Sun, system temperature is expected to increase substantially, resulting in significantly lower data rates. Use semaphores with sufficient integration to counter increased thermal noise. During the 2023 solar conjunction period, for which Mars is behind the solar disk (about one day) or below 0.4 deg (about 2 days), the option of taking a temporary communication outage should be weighed against the expense of inserting a trailing or leading relay satellite into Mars or Earth orbit.

VIII. Conclusion

During the initial phase of the human exploration of Mars, a reliable communications link to and from Earth will be required. Several strategies for obtaining a reliable communications link to Mars have been explored. A significant increase in data return can be realized by going to higher telecommunication link frequencies such as Ka-band, which suffers significantly less solar effects than X-band at the same SEM angle. Other options, such as the use of FSK, frequency semaphores, and spatial and frequency diversity, have been discussed.

Acknowledgments

We would like to thank R. Cesarone and J. Briedenthal for their support of this work; P. Richter for his review and comments; S. Shambayati and A. Kantak for their comments; R. Carnright for Satellite Orbit Analysis Program (SOAP) support; P. Penzo for mission design analysis support; and J. Georgini for providing the ephemeris of Mars that was used to generate plots.

References

[1] R. S. Bokulic and W. V. Moore, "Near Earth Asteroid Rendezvous (NEAR) Spacecraft Solar Conjunction Experiment," *Journal of Spacecraft and Rockets*, vol. 36, no. 1 pp. 87–91, January–February 1999.

[2] Y. Feria, M. Belongie, T. McPheeters, and H. Tan, "Solar Scintillation Effects on Telecommunication Links at Ka-Band and X-Band," *The Telecommunications and Data Acquisition Progress Report 42-129, January–March 1997*, Jet Propulsion Laboratory, Pasadena, California, pp. 1–11, May 15, 1997. http://tmo.jpl.nasa.gov/tmo/progress_report/42-129/129A.pdf

[3] P. E. Beyer, D. J. Mudgway, and M. M. Andrews, "The Galileo Mission to Jupiter: Interplanetary Cruise Post-Earth-2 Encounter Through Jupiter Orbit Insertion," *The Telecommunications and Data Acquisition Progress Report 42-125, January–March 1996*, Jet Propulsion Laboratory, Pasadena, California, pp. 1–16, May 15, 1996.
http://tmo.jpl.nasa.gov/tmo/progress_report/42-125/125B.pdf

[4] D. Morabito, S. Shambayati, S. Butman, D. Fort, and S. Finley, "The 1998 Mars Global Surveyor Solar Corona Experiment," *The Telecommunications and Mission Operations Progress Report 42-142, April–June 2000*, Jet Propulsion Laboratory, Pasadena, California, pp. 1–18, August 15, 2000.
http://tmo.jpl.nasa.gov/tmo/progress_report/42-142/142C.pdf

[5] R. Woo, "Measurements of the Solar Wind Using Spacecraft Radio Scattering Observations," *Study of Traveling Interplanetary Phenomena*, Dordrecht, Holland: D. Reidel Publishing Company, pp. 81–100, 1977.

[6] *Deep Space Mission Systems (DSMS) Telecommunications Link Design Handbook*, 810-005, Rev. E, Module 105, Jet Propulsion Laboratory, Pasadena, California, January 15, 2001.

[7] T. Y. Otoshi, "Measured Sun Noise Temperatures at 32 Gigahertz," *The Telecommunications and Mission Operations Progress Report 42-145,January–March 2001*, Jet Propulsion Laboratory, Pasadena, California, pp. 1–32, May 15, 2001.
http://tmo.jpl.nasa.gov/tmo/progress_report/42-145/145C.pdf

[8] T. A. Rebold, T. K. Peng, and S. D. Slobin, "X-Band Noise Temperature Near the Sun at a 34-Meter High Efficiency Antenna," *The Telecommunications and Data Acquisition Progress Report 42-93, January–March 1988*, Jet Propulsion Laboratory, Pasadena, California, pp. 247–256, May 15, 1988.
http://tmo.jpl.nasa.gov/tmo/progress_report/42-93/93V.PDF

[9] D. Morabito, S. Shambayati, S. Finley, and D. Fort, "The Cassini May 2000 Solar Conjunction," to appear in *IEEE Transactions on Antennas and Propagation*.

[10] B. Rickett, "Interstellar Scattering and Scintillation of Radio Waves," *Annual Review of Astronomy and Astrophysics*, edited by G. Burbidge, D. Layzer, and J. Phillips, vol. 15, Palo Alto, California: Annual Reviews Inc., 1977.